Experimental Analysis and Theoretical Modeling of the Mechanical Behavior of Starch-Grafted-Polypropylene/ Kenaf Fibers Composites

Y.J. Phua,[1,2] A. Pegoretti,[3] Z.A. Mohd Ishak [1,4]

[1]*Cluster for Polymer Composites, Science and Engineering Research Centre, Engineering Campus, Universiti Sains Malaysia, Nibong Tebal, Penang, 14300, Malaysia*

[2]*Physics of Geological Processes, Department of Physics, University of Oslo, Oslo, Norway*

[3]*Department of Industrial Engineering, University of Trento, Trento, 38123, Italy*

[4]*School of Materials and Mineral Resources Engineering, Universiti Sains Malaysia, Nibong Tebal, Penang, 14300, Malaysia*

Mechanical properties of starch-grafted-polypropylene/kenaf fibers (KF) composites were investigated and compared to different theoretical models. In this work, the composites were prepared via melt compounding and compression molding processes at different KF loadings, that is, 10, 20, and 30 wt%. Tensile, fracture toughness and fatigue tests were performed. Generally, the mechanical properties increased with increasing kenaf fiber loadings. This is attributed to the good filler-matrix interactions between KF and starch-grafted-polypropylene, as observed by scanning electron microscopy. Tensile properties were modeled using the rule of mixture, the Kelly-Tyson and the Halpin-Tsai models. Fatigue data were also modeled using different theoretical models to fit both S–N and normalized S–N curves with simple linear model and Boltzmann sigmoidal function. POLYM. COMPOS., 39:3289–3299, 2018. © 2017 Society of Plastics Engineers

INTRODUCTION

Natural fiber has been used extensively in various applications throughout human history. Due to the increased concern in searching a sustainable and ecological technology, substitution of synthetic fibers with natural fibers in producing polymer composites has been a rapidly expanding field of research. Kenaf (*Hibiscus cannabinus*, L. family Malvacea) is one of the most widely used natural fibers in producing polymer composites. Kenaf fibers (KF) are found in the bast (bark) and core (wood), comprising 35% and 65%, respectively. Kenaf bast fiber is a promising candidate to be used in fiber reinforced polymer composites, owing to its superior properties such as excellent tensile strength, as well as high toughness. Furthermore, kenaf has great availability and low material cost in comparison to other natural fibers [1–3]. Numerous researchers have reported on the study of KF reinforced polymer composites using various polymer matrices, such as polypropylene [4–8], starch-grafted polypropylene [9, 10], unsaturated polyesters [11–14], polyurethane [15, 16], epoxy [17, 18], etc.

In recent years, development of biocomposites based on biodegradable polymers and natural fibers is being widely explored, as an effort to reduce the plastic waste problem. KF have been incorporated into different biodegradable polymer matrices, including poly(butylene succinate) [19, 20], cellulose acetate [21], thermoplastic starch [22, 23], poly(lactic acid) [24, 25], etc. However, extensive application of these biodegradable plastics is still hampered by their possible inherent limitations, for instance high cost, poor processability, and tendency to degradation during processing, storage and service. Besides that, there is a strong debate on the recyclability of biodegradable plastics, for which there is no separate recycling stream. Development of hybrid or biphasic polymers based on bio-based polymer and conventional polyolefin (generally polyethylene or polypropylene) appears

Correspondence to: Z. A. Mohd Ishak; e-mail: zarifin@eng.usm.my or zarifin.ishak@gmail.com

Y.J. Phua gratefully acknowledges the financial support from USM Research University Cluster Grant (1001/PKT/8640012) and Erasmus Mundus One More Step mobility grant (2011-2581 001-001 EMA2).
DOI 10.1002/pc.24344
Published online in Wiley Online Library (wileyonlinelibrary.com).

to be a potential solution to overcome the limitations of biodegradable plastics [26].

In this study, a commercialized biphasic thermoplastic, Gaïalene® (supplied by Roquette, France) was used as a matrix to form an environmental friendly composite with short kenaf fibers (SKF). Gaïalene® is a starch-grafted-polypropylene (starch-g-PP) with the starch/polypropylene ratio of 52/48, which is designed for durable and semi-durable uses [9, 26]. According to the manufacturer, it is over 50% bio-based and the production yields a carbon footprint about 65% lower than that of the cleanest fossil polymers. The mechanical performance of Gaïalene® is similar to PP and thus, addition of reinforcement such as natural fibers is essential to further improve its mechanical properties. Addition of natural fibers would also increase the bio-based portion of the material, making it more environmental friendly. Reinforcement effects of KF on the mechanical properties of PP have been widely investigated by numerous researchers [5–8]. However, there is an issue of the compatibility between the hydrophobic PP and the hydrophilic KF. Starch-g-PP is a biphasic polymer consists of both hydrophilic and hydrophobic phases, which favors the dispersion of KF. Therefore, starch-g-PP shows a great potential to be used as a more environmental friendly alternative to the conventional polyolefin, especially in the composite industry. To the best of our knowledge, research on the starch-g-PP/KF composites is not extensively reported in the open scientific literature. In our previous work, we have reported the improvement of tensile properties, hardness, creep stability and tensile impact stress after incorporation of KF into the starch-g-PP [9], along with thermal, rheological, and dynamic mechanical properties [10]. Since there is lack of study on the starch-g-PP/KF composites, a more fundamental study on their mechanical properties is necessary. As an extension of our previous research, this article reports on the fracture toughness, fatigue and biaxial tensile properties of starch-g-PP/SKF composites at various fiber loading. To provide a better understanding on the tensile performance, prediction of tensile properties is performed by applying different theoretical models, that is, rule of mixture (ROM), Kelly-Tyson model and Halpin-Tsai model. Fatigue data are also fitted using different theoretical models. These models were chosen because they are the most commonly used mathematical models to predict tensile and fatigue properties of polymer composites reinforced with discontinuous (short) fibers. It is worthwhile to compare the predictive capabilities of various models, in order to determine the most suitable model to predict the mechanical properties of starch-g-PP/SKF composites.

MODELS FOR TENSILE PROPERTIES PREDICTIONS

The rule of mixtures (ROM) to estimate the properties of composite materials is based on an assumption that the composite property is equal to the sum of the volume-weighted property of its component materials. The ROM is described as the equation below:

$$P_c = P_f v_f + P_m v_m \tag{1}$$

where P_c, P_f, P_m are the material properties of composite, fiber, and matrix, respectively, while v_f and v_m are the volume fractions of fiber and matrix [27, 28]. For short fibers reinforced composites, an orientation factor (η_o) should be taken into account. Therefore, the ROM equation is modified as below [27, 29]:

$$P_c = \eta_0 P_f v_f + P_m v_m \tag{2}$$

The semi-empirical Halpin–Tsai model for the prediction of elasticity of composite material can be expressed as follows [30]:

$$\frac{P_c}{P_m} = \frac{1+\zeta\eta v_f}{1-\eta v_f} \tag{3}$$

with

$$\eta = \frac{(P_f/P_m)-1}{(P_f/P_m)+\zeta} \tag{4}$$

where ζ is a shape-fitting parameters whose value for longitudinally aligned fibers is $\zeta = 2(L/D)$ with L and D being the fiber length and diameter, respectively [27, 29].

The Halpin–Tsai equation was originally used for composites with unidirectional reinforcement. In order to account for the random fiber orientation observed in short fiber composites, Tsai [31] proposed the following empirical equation to predict the elastic modulus of composites containing random-orientated fibers (E_R):

$$E_R = \frac{3}{8}E_L + \frac{5}{8}E_T \tag{5}$$

where E_L and E_T are the longitudinal and transverse moduli of an uniaxially aligned short fiber composites with same fiber aspect ratio and volume fraction. E_L and E_T can be calculated using the Halpin–Tsai equations as below:

$$E_L = E_m \frac{1+\zeta_L\eta_L v_f}{1-\eta_L v_f} \tag{6}$$

and

$$E_T = E_m \frac{1+\zeta_T\eta_T v_f}{1-\eta_T v_f} \tag{7}$$

where E_m is the matrix modulus, ζ and η are expressed as:

$$\zeta_L = 2\frac{L}{D};\ \zeta_T = 2;\ \eta_L = \frac{(E_f/E_m)-1}{(E_f/E_m)+\zeta_L};\ \eta_T = \frac{(E_f/E_m)-1}{(E_f/E_m)+\zeta_T}$$

where L/D is the fiber aspect ratio and E_f is the fiber modulus. Subscripts L and T refer to the longitudinal and

 DOI 10.1002/pc

transverse directions, respectively [9]. Nielsen [32] modified the Halpin–Tsai equations by including a maximum packing fraction, v_r^*:

$$E=E_m\frac{1+\zeta\eta v_f}{1-\eta\Phi v_f} \tag{8}$$

where

$$\Phi=1+\left(\frac{1-v_r^*}{v_r^{*2}}\right)v_f \tag{9}$$

The strength of short fiber composites is often estimated according to the Kelly–Tyson model, which is based on the concept of stress transfer at the fiber–matrix interface. It considers that a constant shear stress is induced from the fiber ends that results in a linear stress built up [33]. Generally, the Kelly–Tyson model can be used to evaluate composite strength (σ_c) using the equation below [34, 35]:

$$\sigma_c=\left[\eta_o\cdot\sum\nolimits_{l_i<l_c}\frac{\tau l_i v_{f,i}}{2r_f}\right]+\left[\eta_o\cdot\sum\nolimits_{l_j>l_c}\sigma_f v_{f,j}\left(1-\frac{l_c}{2l_j}\right)\right]+[\sigma_m(1-v_f)] \tag{10}$$

where η_o is the orientation factor; l_i and l_j are the subcritical (i) and supercritical (j) fiber length; l_c is the critical fiber length; $v_{f,i}$ and $v_{f,j}$ are the volume faction of fibers with l_i and l_j fiber length; τ is the fiber–matrix interfacial shear stress; r_f is the radius of fiber; σ_f is the ultimate stress of fiber; σ_m is the matrix stress at the composite fracture strain; v_f is the volume fraction of fiber.τ is an important property in fiber reinforced composites as it determines the fiber failure mode, that is, by fiber breakage or fiber pull-out. Bowyer and Bader [36] adopted the Kelly–Tyson approach to obtain the τ by analyzing experimental data of mechanical test and fiber length distribution measurements. The basic premise of the Bowyer and Bader model is that at any value of composite strain, ε_c, there is a critical fiber length, l_c [37, 38]:

$$l_c=\frac{E_f\varepsilon_c r_f}{\tau} \tag{11}$$

By modifying Eq. *10*, the stress in composite (σ_c) can be expressed as:

$$\sigma_c=\eta_0(X+Y)+Z \tag{12}$$

where X, Y, and Z are contributions from the fibers of subcritical length, fibers of supercritical length, and matrix to the composite strength, respectively, that is:

$$X=\sum\nolimits_{l_i<l_c}\frac{\tau l_i v_{f,i}}{2r_f} \tag{13}$$

$$Y=\sum\nolimits_{l_j>l_c}E_f\varepsilon_c v_{f,i}\left(1-\frac{E_f\varepsilon_c r_f}{2l_j\tau}\right) \tag{14}$$

$$Z=E_m\varepsilon_c(1-v_f) \tag{15}$$

For the estimation of τ, first, two composite strains were selected from the data of mechanical tests (ε_1 and ε_2) together with their corresponding stress values (σ_1 and σ_2). ε_1 and ε_2 are used to calculate the corresponding matrix contributions, Z_1 and Z_2 using Eq. *15*. The R value was then determined as:

$$R=\frac{\sigma_1-Z_1}{\sigma_2-Z_2} \tag{16}$$

Next, a value of τ was assumed. Using this τ, critical fiber lengths at ε_1 and ε_2 were calculated using *Eq. 11*. Knowing the critical fiber length, X and Y can then be evaluated from Eqs. *13* and *14*, for the whole range of fiber length distributions. Then, R' can be calculated:

$$R'=\frac{X_1+Y_1}{X_2+Y_2} \tag{17}$$

where X_1 and Y_1 corresponding to X and Y values at ε_1, while X_2 and Y_2 corresponding to X and Y values at ε_2. R' value was then compared with R value. If they are different, the assumed τ value is tuned by ±0.1 MPa, and the same procedure repeated until the R' value is approaching the R value. Then, the τ value will be tuned to ±0.01 MPa, until the R' value is equal to the R value, up to four decimal digits. Finally, the equivalent τ value was used to calculate the composite strength using the Kelly-Tyson model (*Eq. 10*).

EXPERIMENTAL

Materials

Starch-g-PP (Gaïalene®, grade G906PJ) with a density of 1.1 g/cm^3 (ISO 1183), a melt flow index of 40 g/10 min (ISO 1133, 190°C, 10 kg) and a melting temperature of 160°C, was supplied by Roquette S.A (Lestrem, France). Short kenaf fibers (SKF, $L/D = 30$) were provided by Kenaf Natural Fibre Industries Sdn. Bhd. (KFI), Malaysia. They are composed of 45–57 wt% of cellulose, 21.5 wt% of hemicelluloses, 8–13 wt% of lignin, and 3–5 wt% of pectin, with an average density of 1.4 g/cm^3 [39].

Composites Preparation

Starch-g-PP pellets and SKF were dried overnight in a vacuum oven at 50°C and 80°C, respectively. Starch-g-PP/SKF composites with different fiber loading (Table 1) were prepared by melt mixing in an internal mixer (Rheomix 600 by Thermo Haake®, Karlsruhe, Germany) with counter-rotating roller rotors. The process was carried out at a temperature of 175°C, rotor speed of 60 rpm and residence time of 7 min. Then, composite sheets were produced by compression molding in a Carver® hydraulic laboratory press at 170°C, followed by fast cooling. Various specimens were punch-cut from the molded sheets. The material compositions and coding are reported in Table 1.

TABLE 1. Material designation and compositions.

Materials designation	Composition	Parts
Gaialene	Starch-g-PP	100
SKF10	Starch-g-PP/short kenaf fibers	90/10
SKF20	Starch-g-PP/short kenaf fibers	80/20
SKF30	Starch-g-PP/short kenaf fibers	70/30

Scanning Electron Microscopy (SEM)

Samples were fractured after immersion for 30 min in liquid nitrogen, and the fracture surfaces were observed by a Zeiss Supra 40 (Carl Zeiss, Berlin, Germany) field emission scanning electron microscope (FESEM) at an accelerating voltage of 3 kV. The samples were sputter-coated with a thin layer of gold to avoid electrical charging during examination.

Tensile Test

Tensile test was performed on ISO 527-2 type 1BA specimens using an Instron model 4502 (Norwood, MA) universal testing machine equipped with a 10 kN load cell. An axial extensometer (Instron, model 2620) with a gauge length of 12.5 mm was attached to the specimens to measure the strain values up to 2% at a cross-head speed of 1 mm/min. According to ISO 527 standard, the elastic modulus was evaluated as a secant value between deformation levels of 0.05% and 0.25%. With an additional transversal extensometer (Instron, model 2640) attached during the tensile test, Poisson's ratio was evaluated as a ratio of transverse contraction strain to longitudinal extension strain in the direction of stretching force. Tensile test up to fracture was performed at a higher cross-head speed (10 mm/min) without the extensometer. Tests were performed at room temperature on five specimens for each sample.

Fracture Toughness Test

Single edge notched bending (SENB) test was conducted according to ASTM D5045-99 standard using an Instron model 4502 (Norwood, MA) universal testing machine at a cross-head speed of 10 mm/min and span length of 40 mm. The specimens dimension were $10 \times 60 \times 4$ mm^3 with a sharp notch of initial length of 5 mm. Tests were performed at room temperature on five specimens for each sample.

Fatigue Test

Fatigue test was carried out according to ASTM D3479 standard using a closed loop servo hydraulic MTS 858 Mini Bionix testing machine. A 10-Hz sinusoidal stress ranging from a minimum (σ_{min}) stress up to a maximum (σ_{max}) stress, that is, 25%–90% of the quasi-static strength was applied. A load ratio $R = \sigma_{min}/\sigma_{max}$ of 0.1 was fixed for all tests. Fatigue cycles were recorded up to a maximum number of 500,000.

RESULTS AND DISCUSSION

Morphological Properties

SEM micrographs of cryofractured cross-section surface of Gaialene and its composites are shown in Fig. 1.

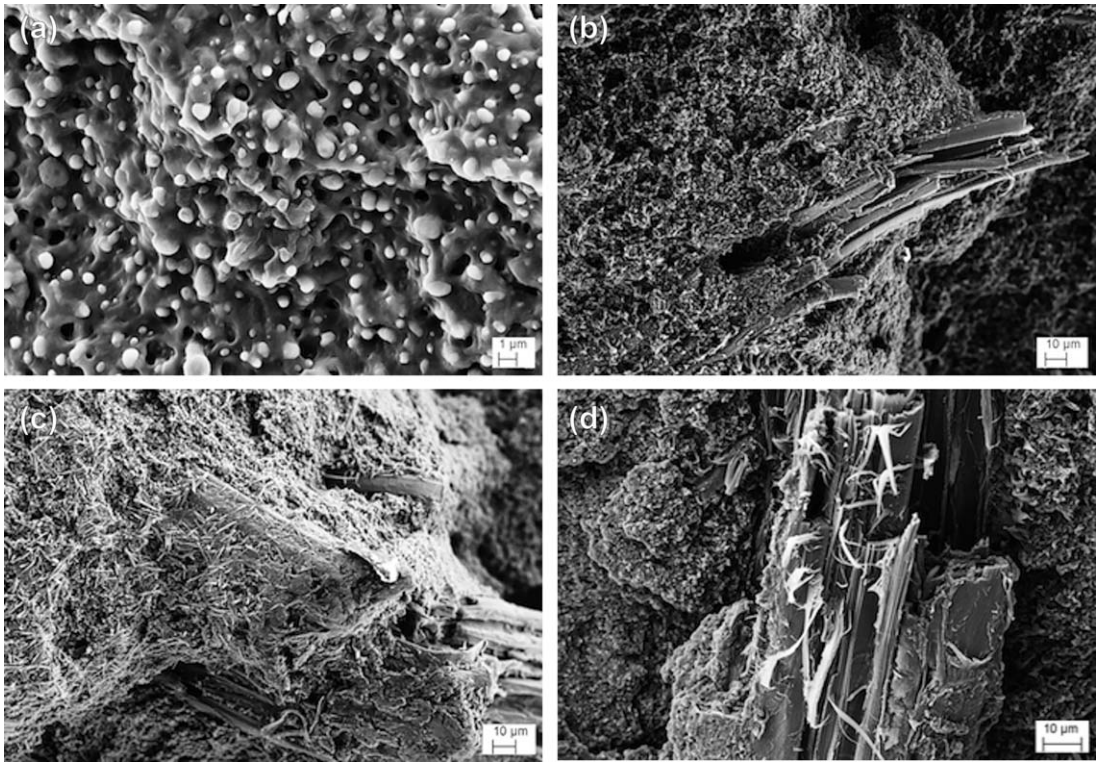

FIG. 1. SEM micrographs of (a) Gaialene, (b) SKF10, (c) SKF20, and (d) SKF30.

 DOI 10.1002/pc

TABLE 2. Tensile properties of Gaialene and its composites.

Compound	Modulus (GPa)	Tensile stress at yield (MPa)	Tensile strain at yield (%)	Tensile stress at break (MPa)	Elongation at break (%)	Poisson's ratio
Gaialene	1.11 ± 0.11	20.7 ± 2.7	3.52 ± 0.54	19.5 ± 2.7	4.90 ± 1.7	0.45 ± 0.03
SKF10	2.01 ± 0.42	–	–	21.1 ± 4.5	1.88 ± 0.01	0.45 ± 0.09
SKF20	3.47 ± 1.20	–	–	22.8 ± 3.2	1.46 ± 0.60	0.65 ± 0.22
SKF30	4.92 ± 1.00	–	–	23.2 ± 3.3	0.83 ± 0.36	0.73 ± 0.13

Two distinct phases are clearly noticeable in the biphasic neat Gaialene matrix, as shown in Fig. 1a. The continuous phase is PP, while the dispersed phase is thermoplastic starch (TPS) that appears as particles with diameters in the range from 0.2 up to 1.5 μm. It can be seen that TPS particles are homogenously dispersed in the PP matrix, and both phases are well bonded to each other. This is in line with the observations reported by Hamma et al. [9] and Tessier et al. [26].

Figure 1b–d shows the cross-section surface of kenaf-reinforced composites at different fiber loading. For all composites, no gaps are observed at the interface between KF and Gaialene matrix, which reveals a good interfacial wettability. The good compatibility between them could be attributed to the chemical affinity between TPS component in Gaialene and KF. In fact, both constituents contain hydroxyl groups and ether links in the glucose units and polysaccharides, which might enable the formation of hydrogen bonds [9].

Tensile Properties

Tensile Modulus. Tensile properties of Gaialene and its composites are presented in Table 2. Tensile modulus is significantly increased with the presence of KF with an increment of 81%, 213%, and 343% at 10, 20, and 30 wt% of fiber loading, respectively. It is well documented that, due to its relative high tensile modulus (~53 GPa), KF notably increases the tensile modulus of most polymer matrices [3, 9, 39].

The experimental data are here compared with the values predicted using different mathematical equation based on ROM, Kelly-Tyson and Halpin–Tsai models. Figure 2 presents the tensile moduli predicted using the ROM (Eq. *2*) at different orientation factors (η_o). The ROM is the simplest mechanical model to estimate the properties of a multiple component system such as composite. According to the literature, a three-dimensional (3-D) random fiber alignment yields a η_o of 0.2, a planar random fiber arrangement yields a η_o of 0.375, while an uniaxial-aligned fiber arrangement yields a η_o of 1 [40]. Schematic diagram of different fiber orientations is illustrated in Fig. 3. The original ROM (Eq. *1*) assumes all fibers are uniaxial-aligned ($\eta_o = 1$), which is untrue for most of the short fibers reinforced composites. This can be clearly seen from Fig. 2 that the experimental tensile moduli are markedly deviate from the values predicted using the original ROM. However, it is interesting to observe that the experimental data can be very well fitted with the ROM model at η_o of 0.2. This suggests that KF in these composites are aligned in a 3-D random orientation, especially at 10 wt%. As fiber loading is increased to 20 and 30 wt%, the tensile modulus values situated between $\eta_o = 0.375$ and $\eta_o = 0.2$. The fiber alignment shows tendency of shifting from 3-D random to planar random alignment as the fiber loading is increased. At low fiber loading, there is sufficient space in the composite for KF to be dispersed in all directions and form a 3-D random fiber orientation. Meanwhile, there is limited space for the dispersion of fibers at high fiber loading. This increases fiber–fiber contact, subsequently increases the tendency of fibers to be dispersed as a stack of 2-D random networks in a single plane (planar random).

The most common model that is used to predict Young's modulus of short fiber-reinforced polymer composites is the Halpin–Tsai model [30]. In this work, tensile moduli are modeled using an empirical equation (*Eq. 5*) that is based on the Halpin–Tsai equations. Besides that, tensile moduli are also modeled using the modified Halpin–Tsai equations proposed by Nielsen [32], which include the maximum packing fraction, v_r^* as presented in Eq. *8*. According to Nielsen [32], v_r^* is highly dependent on the filler type and the filler arrangement in the composite. For fibrous reinforcements, $v_r^* = 0.785$ if they are arranged in a uniaxial simple cubic packing, $v_r^* = 0.9065$ if they are arranged in a uniaxial hexagonal close packing, $v_r^* = 0.82$ if they are arranged in uniaxial random close packing, while $v_r^* = 0.52$ if they are arranged in a 3-

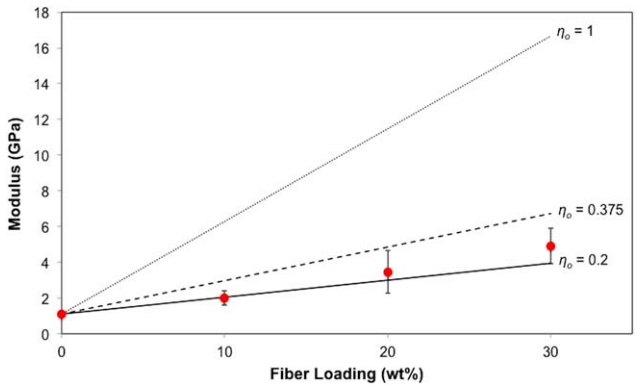

FIG. 2. Experimental (•) and theoretical (lines) tensile moduli predicted using the ROM at different orientation factor (η_o). [Color figure can be viewed at wileyonlinelibrary.com]

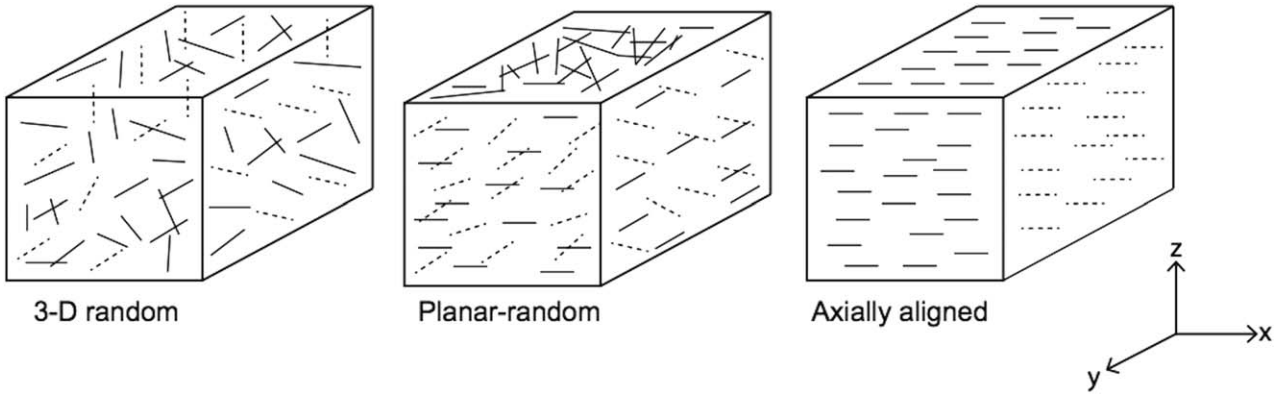

FIG. 3. Schematic diagram of different fiber orientations.

D random packing [41, 42]. According to observations from the ROM model, KF in these composites are aligned in a 3-D random orientation. Therefore, in our case, $v_r^* = 0.52$ is used.

Figure 4 shows the experimental and theoretical tensile moduli predicted using the Halpin–Tsai model (Fig. 4a) and the modified Halpin–Tsai model proposed by Nielsen [32] (Fig. 4b) at different fiber aspect ratios (*L*/*D*). Volume fractions were used in the calculations but the results are presented in weight fractions, which is in line with the experimental method that we used. Aspect ratio of fibers after processing can also be predicted from the plots, by comparing the experimental values with the corresponding aspect ratios from the theoretical line plots. From Fig. 4a, it can be seen that tensile moduli predicted by Halpin–Tsai model are not very well fitted to the experimental values at high fiber loading (20 and 30 wt%). The experimental tensile moduli of SKF20 and SKF30 are found to be approximately situated at *L*/*D* of 30. Based on our previous study on the fiber length distribution reported by Hamma et al. [9], the average aspect ratio of KF decreased after processing from the initial values of 30 to around 18. In fact, fiber aspect ratio after processing will not be the same as its initial aspect ratio due to the fiber breakage during mixing and molding processes. Hence, the aspect ratio of 30 for SKF20 and SKF30 composites that predicted by the Halpin–Tsai model is inaccurate. Besides that, the high standard deviations of the experimental results may also be one of the reasons for the poor agreement of the experimental results with the theoretical predictions. However, the modified Halpin–Tsai model that includes the maximum packing fraction demonstrates good agreement with the experimental results, as shown in Fig. 4b. The corresponding theoretical aspect ratios of KF are positioned between L/D of 18-26, which is in good agreement with the experimental fiber aspect ratio [9]. This implies that the Halpin–Tsai model gives better estimations after including the maximum packing fraction.

Tensile Strength. Tensile strength values of Gaialene and its composites are reported in Table 2. For neat Gaialene matrix, the failure under tension was preceded by plastic deformation (a yield stress was detected), while only stress at break was detected for the composites. This shows that the fracture behavior changed from ductile to brittle after addition of KF. The main reason of the ductile-to-brittle transition is attributed to the reduction of the molecular mobility constrained by the KF [9]. On the other hand, addition of KF gives positive effects to the tensile strength. Tensile stress at break is increased by 8.2%, 16.9%, and 19% at the KF loadings of 10, 20, and 30 wt%, respectively. The remarkable increase of tensile strength is a clear indication of a good fiber–matrix stress transfer. This is in line with the SEM observations that

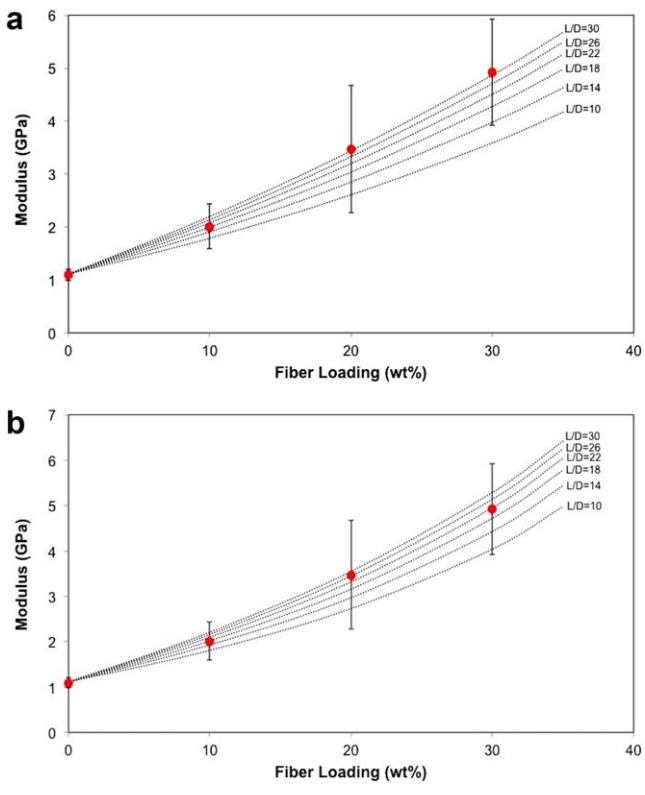

FIG. 4. Experimental (•) and theoretical (lines) tensile moduli predicted using (a) the Halpin–Tsai model and (b) the modified Halpin-Tsai model proposed by Nielsen [32] with $v_r^* = 0.52$ at different fiber aspect ratios (*L*/*D*). [Color figure can be viewed at wileyonlinelibrary.com]

 DOI 10.1002/pc

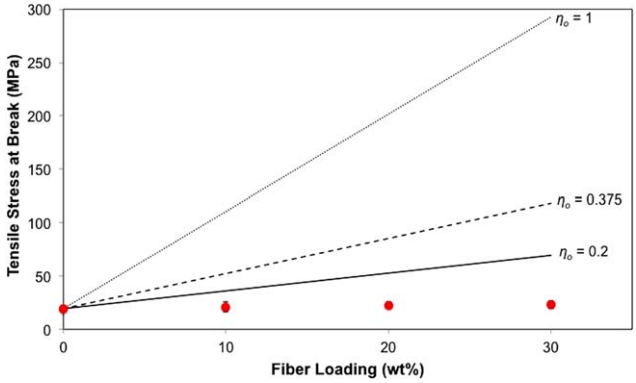

FIG. 5. Experimental (•) and theoretical (lines) tensile stress at break predicted using the ROM at different orientation factor (η_o). [Color figure can be viewed at wileyonlinelibrary.com]

have been discussed earlier, which reveals a strong interfacial interaction and adhesion between KF and Gaialene.

Tensile stress at break of the composites is modeled using the ROM at different orientation factors (η_o), as presented in Fig. 5. It is obvious that the ROM overestimate the composite strength, in fact the experimental results are significantly lower than the theoretical predictions.

The Kelly–Tyson model (Eq. *10*) was also used to evaluate the tensile stress at break. It is often reported as the optimum model to predict the strength of discontinuous fiber composites [37, 38]. Fiber-matrix interfacial shear stress (τ), a parameter required by the model, was determined by analyzing the experimental data of mechanical test and fiber length distribution, as described in the previous section (Eqs. 11-17). The fiber length distribution data reported in our previous publication [9] were used in this calculation. The τ parameter for SKF10, SKF20, and SKF30 composites are 16.4, 32.9, and 31.9 MPa, respectively. This corresponds to critical fiber length (l_c) values of 1.52, 0.59, and 0.34 mm, respectively, for SKF10, SKF20, and SKF30 composites, as calculated from Eq. *11*. τ is inversely proportional to l_c, so short l_c indicates good adhesion. The results show that the fiber–matrix adhesion is better at high fiber loading (20 and 30 wt%). The l_c is the minimum fiber length required to strengthen a material to their maximum potential. Fibers with lengths lower than l_c (subcritical fibers) are too short to support the load to cause fiber fracture. Thus, fiber pull-out and matrix fracture are the main failure mechanisms in the composite. For fibers with lengths longer than l_c (supercritical fibers), fiber fracture will be the dominating mechanism during fracture of composite [36, 38]. The average fiber length of KF in the composites is 0.6 mm [9]. Hence, it is anticipated that the fracture of SKF10 composite is dominated by fiber pull-out and matrix fracture because most of the fibers are shorter than l_c (1.52 mm). For SKF20 and SKF30 composites, most of the fibers in the composites are equal to or longer than their l_c. Thus, they show better tensile strength than the SKF10 composite because the applied load is carried by most of the fibers.

Using the obtained τ and l_c values, Kelly–Tyson model (Eq. *10*) was applied to evaluate the theoretical tensile stress at break, and the results are illustrated in Fig. 6. The tensile stress at break predicted by Kelly–Tyson model shows a good fit with the experimental results. In addition, it can be seen that the fiber alignment shows tendency of shifting from 3-D random to planar random alignment as the fiber loading is increased. This is in good agreement with our tensile modulus predictions using the ROM, which has been discussed earlier (Fig. 2). In short, the Kelly–Tyson model is a better model to predict tensile strength, than the ROM.

Elongation at Break. From Table 2, it is noted that the elongation at break decreased remarkably with the fiber loading. It is understandable that the incorporation of KF with a relatively low elongation at break (1.6%) [3] to the Gaialene will reduce the overall elongation at break.

Poisson's Ratio. From Table 2, it can be observed that the Poisson's ratio of composites remained unchanged at 10 wt% KF loading, but increased to 0.65 and 0.73 at 20 and 30 wt% of fiber loading, respectively. Theoretically, Poisson's ratio of a stable and isotropic material in three dimensions cannot be less than −1.0 nor greater than 0.5 [43, 44]. In our case, Poisson's ratios of SKF20 and SKF30 are greater than 0.5. This illustrates a possible anisotropic behavior of the composites, due to the alignment of fibers. According to the theoretical models that have been discussed earlier, the fiber alignment shows tendency of shifting from 3-D random to planar random alignment at SKF20 and SKF30 composites. The Poisson's ratio results have further strengthened this statement. KF tend to arrange in a 2-D planar random alignment at 20 and 30 wt% fiber loading, which increased the anisotropy of the composites. Similar observations are also reported by Lee and Lakes [44], which observed a Poisson's ratio greater than 1 for an

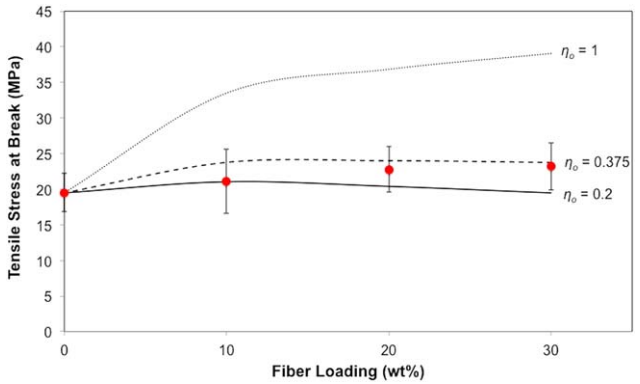

FIG. 6. Experimental (•) and theoretical (lines) tensile stress at break predicted using the Kelly–Tyson model at different orientation factor (η_o). [Color figure can be viewed at wileyonlinelibrary.com]

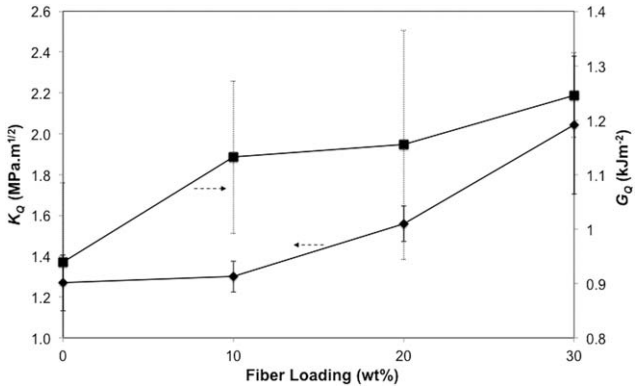

FIG. 7. Critical stress intensity factor, K_Q (υ) and critical energy release rate, G_Q (ν) as a function of kenaf fiber loading.

anisotropic polyurethane foam. Peel [45] also explained that there is no theoretical limit of Poisson's ratio for anisotropic materials.

Fracture Toughness

From the SENB test, fracture toughness is calculated according to the ASTM D5045-99 standard. Certain samples failed to meet the size requirements set in ASTM D5045-99 to provide a valid fracture toughness (K_{IC}). In fact, for a valid K_{Ic} test it is required that the material behavior is essentially linear elastic, with the plastic zone size at the crack tip small enough to be ignored [46]. Therefore, fracture toughness values obtained on these materials are reported as apparent fracture toughness values [46–48].

Figure 7 presents the apparent fracture toughness of Gaialene and its composites, in terms of the apparent values of both the critical stress intensity factor (K_Q) and the critical strain energy release rate, (G_Q). The relationship between K_Q and G_Q is expressed as $K_Q^2 = G_Q\ E'$, with $E' = E$ for plane stress and $E' = E/(1\text{-}v^2)$ for plane strain condition, where E is the Young's modulus, and v is the Poisson's ratio of the material [48–50]. From Fig. 7, it can be seen that the apparent fracture toughness increased with the KF loading. This indicates that addition of KF into Gaialene has contributed to toughening the material. In general, there are several mechanisms that can contribute to the toughness of fiber-reinforced composites. Fiber debonding, friction, and fiber fracture give significant contributions to energy dissipation during composite fracture [51]. Fibers can act as obstacles, leading to crack deflection because cracks tend to propagate by twisting around the fiber. Larger fracture energy is required to overcome the increasing surface area in the system. Friction at the fiber–matrix interfacial region during fiber pull-out also increased the energy dissipation. Besides that, the SEM micrographs (Fig. 1) show a good adhesion between the KF and the Gaialene matrix. Therefore, the applied stress can be transferred efficiently from the composite matrix to the fibers, rendering the crack initiation more difficult, and subsequently increasing the fracture toughness [52].

Fatigue Behavior

Results from fatigue test are plotted as maximum applied stress (σ_{max}) versus cycles to failure (N), as shown in Fig. 8 in a double logarithmic scale, which are commonly known as the S–N curves. In this work, tensile stress was applied from 90% of the quasi-static strength and reduced in steps of 10% until specimens survived 500,000 cycles. Therefore, fatigue limit in this work refers to the stress level for which specimen lasted for at least 500,000 cycles. From Fig. 8, it is obvious that the KF-reinforced composites show a higher fatigue limit than the neat Gaialene, and the fatigue limit improved as the KF loading increased. This can be correlated to the better tensile properties of KF-reinforced composites as compared to the neat Gaialene, which lead to the better fatigue performance. This result once again proves the reinforcing effects of KF to the Gaialene matrix.

S–N curve is the main basic tool to analyze and predict fatigue lifetime of a material. According to the literature [53, 54], fatigue data can be fitted using a theoretical model as shown in the following equation:

$$\sigma_{max} = BN^{(-1/k)} \tag{18}$$

where B and k are material constants. From the linear regression of fatigue data of Fig. 8, the square of correlation coefficient (R^2) can be determined, which quantitatively indicates the goodness of fit between the regression and the data [54]. The fitting parameters B and k and R^2 values are reported in Table 3. The parameter k can be used to evaluate the fatigue resistance of a material [53]. A high k value shows a high fatigue limit of the material, which means that the material is less sensitive to fatigue failure. Table 3 shows that the k values increased as KF loading increased in the composites, reflecting a higher fatigue limit at high KF loading.

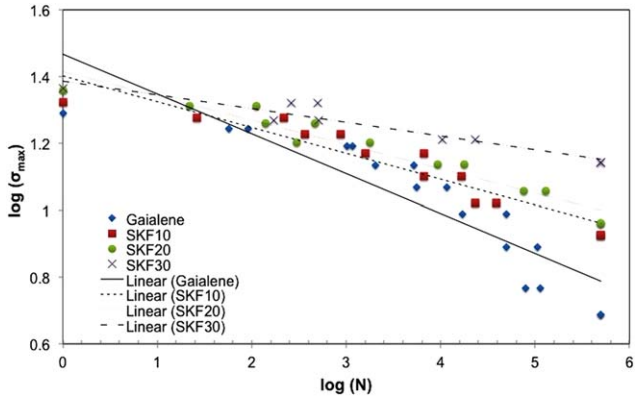

FIG. 8. S–N curves in log–log scale with the fitting lines. [Color figure can be viewed at wileyonlinelibrary.com]

 DOI 10.1002/pc

TABLE 3. Constant values and fitting parameters.

	Eq. *18*			Eq. *19*		*Eq.* 20				
Sample	*B*	*k*	R^2	*m*	R^2	A_1	A_2	N_o	*dN*	R^2
Gaialene	29.29	8.42	0.813	0.115	0.843	0.978	0.052	4.926	0.551	0.978
SKF10	25.23	12.95	0.893	0.098	0.900	0.978	0.306	4.593	0.452	0.986
SKF20	26.78	13.62	0.913	0.096	0.934	0.998	0.306	4.638	0.452	0.986
SKF30	24.56	23.92	0.921	0.068	0.916	0.980	0.563	4.291	0.437	0.990

Normalized S–N curves in semi-log scale of the fatigue data are presented in Fig. 9. Several models can be employed on these curves to model the fatigue behavior of short fiber composites. The most popular model is a simple linear model represented by the following equation [53, 55, 56]:

$$\frac{\sigma_{\max}}{\sigma_b} = 1 - m\log(N) \tag{19}$$

where σ_b is the tensile stress at break as obtained from the tensile test, and *m* is a fitting constant. Fig. 9a shows the linear regression of the experimental data using Eq. *19*, while the fitting parameter and the correlation coefficient are reported in Table 3. According to Tate et al. [56], a low value of *m* indicates a higher fatigue strength.

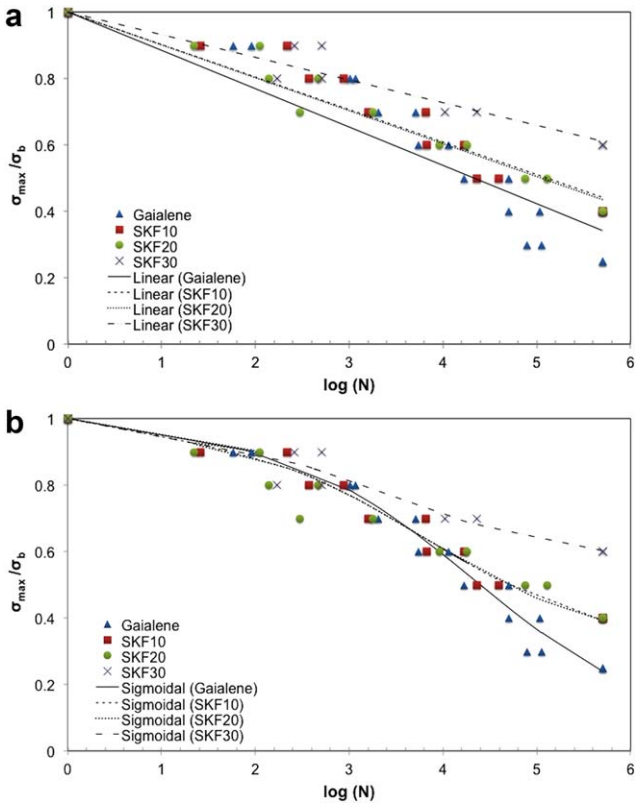

FIG. 9. Normalized S–N curves in semi-log scale with the fitting lines according to (a) Eq. *19* and (b) Eq. *20*. [Color figure can be viewed at wileyonlinelibrary.com]

Hence, the *m* values obtained from the model indicates that fatigue strength of the material improves with the KF loading, in good agreement to the observation of fatigue strength as discussed earlier. Based on the R^2 values obtained from curve fitting by Eqs. *18* and *19*, there is no clear advantage in choosing either of these models. Besides that, the fatigue data can also be modeled using a nonlinear curve fitting model based on the Boltzmann sigmoidal function [53, 56]:

$$\frac{\sigma_{\max}}{\sigma_b} = \frac{A_1 - A_2}{1 + e^{(\log N - \log N_o)/dN}} + A_2 \tag{20}$$

where A_1 and A_2 represent the upper and the lower fatigue stress limits adopted in the fatigue test, respectively, while N_o is the fatigue life for a stress equal to $(A_1+A_2)/2$ and *dN* describes the steepness of the curve. In this work, the parameters A_1, A_2, N_o, and *dN* were evaluated using the Solver Add-in of Microsoft Excel to fit the data until a minimum R^2 value is reached. The R^2 values and the fitting parameters are listed in Table 3. From Fig. 9b, it can be observed that the Boltzmann sigmoidal function shows the best fit in modeling the fatigue behavior. This also shows that the relationship between the applied stress and the cycles to failure is nonlinear. Furthermore, the goodness of fit of the Boltzmann sigmoidal function is also presented by the high R^2 values close to 1.0. The A_2 values are often used as an indicator of the fatigue limit of the material. The higher A_2 values at higher KF loadings indicate a better fatigue life. Based on the R^2 values, it can be concluded that fatigue behavior can be best modeled using the Boltzmann sigmoidal function.

CONCLUSIONS

Tensile modulus is significantly improved by the addition of KF into the Gaialene matrix. Tensile modulus can be modeled using the rule of mixtures (ROM), the Halpin–Tsai model, and the Halpin–Tsai model including the maximum packing fraction that manifested the better fitting capabilities showed the best fit. Tensile stress at break, fracture toughness, and the fatigue limit were improved by the incorporation of KF, and increased with the KF loadings. This is attributed to the good filler-matrix interactions between Gaialene and KF, as confirmed from the SEM images. The ROM does not show a good fit to predict the tensile stress at break. Tensile

stress at break was better predicted using the Kelly–Tyson model. Besides that, fiber alignment shows tendency of shifting from 3-D random to planar random alignment as the fiber loading is increased, which was revealed by both the ROM and the Kelly–Tyson mechanical model. The fatigue behavior had also proven the reinforcing efficiency of KF in the Gaialene matrix. By comparing the goodness of fit of different models, fatigue behavior can be best modeled using the Boltzmann sigmoidal function. This indicates a nonlinear relationship between the applied stress and the cycles of failure.

REFERENCES

1. P. Russo, C. Carfagna, F. Cimino, D. Acierno, and P. Persico, *Adv. Polym. Tech.*, **32**, 313 (2013).
2. N. Saba, M.T. Paridah, and M. Jawaid, *Constr. Build. Mater.*, **76**, 87 (2015).
3. H.M. Akil, M.F. Omar, A.A.M. Mazuki, S. Safiee, Z.A.M. Ishak, and A. Abu Bakar, *Mater. Des.*, **32**, 4107 (2011).
4. T.T. Law, and Z.A.M. Ishak, *J. Appl. Polym. Sci.*, **120**, 563 (2011).
5. D. Feng, D.F. Caulfield, and A.R. Sanadi, *Polym. Compos.*, **22**, 506 (2001).
6. A. Hao, Y. Chen, and J.Y. Chen, *J. Appl. Polym. Sci.*, **131**, 8864–8874 (2014).
7. N. Sallih, P. Lescher, and D. Bhattacharyya, *Compos. Part A*, **61**, 91 (2014).
8. M. Zampaloni, F. Pourboghrat, S.A. Yankovich, B.N. Rodgers, J. Moore, L.T. Drzal, A.K. Mohanty, and M. Misra, *Compos. Part A*, **38**, 1569 (2007).
9. A. Hamma, M. Kaci, Z.A. Mohd Ishak, and A. Pegoretti, *Compos. Part A*, **56**, 328 (2014).
10. A. Hamma, M. Kaci, Z. Mohd Ishak, R. Ceccato, and A. Pegoretti, *J. Reinf. Plast. Compos.*, **34**, 2045 (2015).
11. S. Misri, S.M. Sapuan, Z. Leman, and M.R. Ishak, *Mater. Des.*, **65**, 953 (2015).
12. J.P. Siregar, T. Cionita, D. Bachtiar, and M.R. Mat Rejab, *Appl. Mech. Mater.*, **695**, 159 (2015).
13. M.P. Bin Saiman, M.S. Bin Wahab, and M.U. Bin Wahit, *Appl. Mech. Mater.*, **465-466**, 962 (2014).
14. A.R. Rozyanty, M.Y. Nur Firdaus, M.A.A. Mohd Salleh, and L. Musa, *Adv. Mater. Res.*, **795**, 631 (2013).
15. M. Nar, C. Webber, and N.A. D'Souza, *Polym. Eng. Sci.*, **55**, 132 (2014).
16. Y.A. El-Shekeil, S.M. Sapuan, K. Abdan, and E.S. Zainudin, *Mater. Des.*, **40**, 299 (2012).
17. D. Ariawan, Z.A.M. Ishak, R.M. Taib, M.Z.A. Thirmizi, and Y.J. Phua, *Adv. Mater. Res.*, **1024**, 267 (2014).
18. Z.N. Azwa, and B.F. Yousif, *Polym. Degrad. Stab.*, **98**, 2752 (2013).
19. M.Z.A. Thirmizir, Z.A.M. Ishak, R.M. Taib, S. Rahim, and S.M. Jani, *J. Appl. Polym. Sci.*, **122**, 3055 (2011).
20. J.M. Lee, Z.A. Mohd Ishak, R. Mat Taib, T.T. Law, and M.Z. Ahmad Thirmizir, *J. Polym. Environ.*, **21**, 293 (2013).
21. C. Pang, R.A. Shanks, and F. Daver, *AIP Conf. Proc.*, **1593**, 350 (2014).
22. R. Moriana, F. Vilaplana, S. Karlsson, and A. Ribes-Greus, *Compos. Part A*, **42**, 30 (2011).
23. A.R.N. Humairah, A. Zuraida, S. Norshahida, and A.W.N. Izwah, *Adv. Environ. Biol.*, **8**, 765 (2014).
24. R.M. Taib, H.M. Hassan, and Z.A. Mohd Ishak, *Polym. Plast. Technol. Eng.*, **53**, 199 (2014).
25. N. Graupner, and J. Müssig, *J. Biobased Mater. Bio.*, **6**, 500 (2012).
26. R. Tessier, E. Lafranche, and P. Krawczak, *Express Polym. Lett.*, **6**, 937 (2012).
27. R. Gibson, Principles of Composite Material Mechanics, CRC Press, New York (2007).
28. K. Friedrich, S. Fakirov, Z. Zhang, Polymer Composites: From Nano- to Macro-Scale, Springer, USA (2005).
29. S. Migneault, A. Koubaa, F. Erchiqui, A. Chaala, K. Englund, and M. Wolcott, *Wood Sci. Technol.*, **45**, 521 (2011).
30. J.C.H. Affdl, and J.L. Kardos, *Polym. Eng. Sci.*, **16**, 344 (1976).
31. P. N. Tsai SW, Invariant Properties of Composite Materials, Technomic Publishing Company, Lancaster (1968).
32. L.E. Nielsen, *J. Appl. Phys.*, **41**, 4626 (1970).
33. R. W. T. A. Kelly, Fiber Strengthened Materials, Wiley, New York (1965).
34. E. Lafranche, V.M. Oliveira, C.I. Martins, and P. Krawczak, *J. Compos. Mater.*, **49**, 113 (2015).
35. A. Kelly, and W.R. Tyson, *J. Mech. Phys. Solids*, **13**, 329 (1965).
36. W.H. Bowyer, and M.G. Bader, *J. Mater. Sci.*, **7**, 1315 (1972).
37. A. Hassan, R. Yahya, M.I.M. Rafiq, A. Hussin, M.R.K. Sheikh, and P.R. Hornsby, *J. Reinf. Plast. Compos.*, **30**, 1233 (2011).
38. T.T. Law, Y.J. Phua, R. Senawi, A. Hassan, and Z.A. Mohd Ishak, *Polym. Compos.*, **37**, 1238–1248 (2016).
39. H. Ku, H. Wang, N. Pattarachaiyakoop, and M. Trada, *Compos. Part B*, **42**, 856 (2011).
40. G.W. Beckermann, and K.L. Pickering, *Compos. Part A*, **40**, 210 (2009).
41. P. K. Mallick, Fiber-Reinforced Composites: Materials, Manufacturing, and Design, 2nd ed., CRC Press, USA (1993).
42. T.B. Lewis, and L.E. Nielsen, *J. Appl. Polym. Sci.*, **14**, 1449 (1970).
43. H. Gercek, *Int. J. Rock Mech. Min. Sci.*, **44**, 1 (2007).
44. T. Lee, and R.S. Lakes, *J. Mater. Sci.*, **32**, 2397 (1997).
45. L.D. Peel, *Phys. Status Solidi (b)*, **244**, 988 (2007).
46. B. Gludovatz, S.E. Naleway, R.O. Ritchie, and J.J. Kruzic, *Acta Mater.*, **70**, 198 (2014).
47. S. Liu, and Y.J. Chao, *Int. J. Fract.*, **124**, 113 (2003).
48. A. Pegoretti, and A. Penati, *Polymer*, **45**, 7995 (2004).
49. J. Gao, J. Li, S. Zhao, B.C. Benicewicz, H. Hillborg, and L.S. Schadler, *Polymer*, **54**, 3961 (2013).
50. Standard Test Method for Fracture Toughness and Strain Energy Release Rate of Plastic Materials (ASTM D5045-99), American Society for Testing and Materials (1999).
51. J. Botsis, and C. Beldica, *Int. J. Fract.*, **69**, 27 (1994).

52. R.V. Silva, D. Spinelli, W.W. Bose Filho, S. Claro Neto, G.O. Chierice, and J.R. Tarpani, *Compos. Sci. Technol*., **66**, 1328 (2006).
53. A. Dorigato, and A. Pegoretti, *J. Compos. Mater*., **46**, 1773 (2012).
54. H.C. Tang, T. Nguyen, T-j. Chuang, J. Chin, J. Lesko, and H.F. Wu, *J. Mater. Civ. Eng*., **12**, 97 (2000).
55. J. F. Mandell, in Chapter 7 - Fatigue Behavior of Short Fiber Composite Materials, Reifsnider, K. L. Ed., Elsevier, **231**, Amsterdam (1991).
56. J.S. Tate, A.D. Kelkar, and J.D. Whitcomb, *Int. J. Fatigue*, **28**, 1239 (2006).